Study of the Transient Behavior of Detached Plasma during Xe Gas Injection into the D-Module of GAMMA 10/PDX

Md. Shahinul ISLAM, Yousuke NAKASHIMA[1)], Takaaki IIJIMA[1)], Kunpei NOJIRI[1)], Naomichi EZUMI[1)], Masayuki YOSHIKAWA[1)], Tsuyoshi KARIYA[1)], Ryutaro MINAMI[1)], Mafumi HIRATA[1)], Kazuo HOSHINO[2)], Akiyoshi HATAYAMA[2)], Hiroki HASEGAWA, Seiji ISHIGURO, Hiroto MATSUURA[3)] and Mizuki SAKAMOTO[1)]

National Institute for Fusion Science, Toki, Gifu 509-5292, Japan
[1)]*Plasma Research Center, University of Tsukuba, Tsukuba, Ibaraki 305-8577, Japan*
[2)]*Graduate School of Science and Technology, Keio University, Hiyoshi, Yokohama 223-8522, Japan*
[3)]*Radiation Research Center, Osaka Prefecture University, Osaka 599-8570, Japan*

(Received 12 July 2020 / Accepted 6 September 2020)

The transition phenomenon of detached plasma during additional heating effects has been studied by applying a short pulse (25 ms) of Electron Cyclotron Heating (ECH) at the east plug-cell of the tandem mirror device GAMMA 10/PDX. In this paper, the plasma parameters on the target plate of the D-module are studied for understanding the impact of transient heating pulse on the sustainability of the detached plasma. The heat flux increases on the target plate for the additional heating case in comparison to without heating pulse. The ion flux also increases when the ECH heating is activated. The electron density enhances significantly during the ECH heating pulse application period. Furthermore, the electron density and the ion flux increase according to the increment of Xe plenum pressure in the case of ECH heating condition. The experimental results clarified that ECH heating pulse can drive the detachment state to attached state in spite of strong effect of Xe gas for generating the detached plasma.

Keywords: GAMMA 10/PDX, D-module, heat flux, ion flux, electron density, detached to attached transition

DOI: 10.1585/pfr.15.1402074

1. Introduction

The control of heat-load on the divertor target plate is an urgent research issue for advancing nuclear fusion research. The high heat-flux enters into the divertor region and strikes on the target plates. Thus, it is necessary to minimize the power load on the divertor target plates. The detached plasma state is considered to be of the promising ways to shield the divertor target plates from the high heat load [1]. The behavior of plasma and neutral particles in the divertor region have been extensively studied in order to understand the divertor plasma physics [1–5]. Neutral particles (recycled or/and externally seeded) play a driving role to generate and sustain the detached plasma. The energy loss processes due to plasma-neutral interactions must be clarified for understanding the divertor physics. Furthermore, the behavior of detached plasma during transient heating condition is an urgent research issue. Therefore, the sustainment of detached plasma during an additional heating case is also an important research subject for divertor plasma physics.

The atomic processes of impurity particles play a key role for reducing the plasma energy. More specifically, radiator gas puffing into the divertor is one of the possible concepts for mitigating the heat and ion fluxes on the target plates because of the radiation cooling effect of the radiator gas, which significantly enhances the electron energy loss terms by enhancing the ionization loss and the radiation loss. Hence, the radiator gases can be introduced into the divertor region for radiative plasma cooling purposes.

The reaction rate co-efficient of radiation cooling of the gases is different. Consequently, it is also necessary to explore the effects of the radiator gases on the plasma detachment. In particular, ionization, excitation, and radiation cooling are the main energy loss channels. The ionization and excitation potential of Xe are low. Hence, Xe can be easily ionized by low energy electrons. Consequently, Xe may be useful for reducing the electron energy. If much higher-energy electrons are entering the Xe environment, multiple ionized ions should be produced in large numbers, which will indicate the good loss channel for electrons. In other words, Xe has more electrons than the other noble gases and may produce many more low energy electrons to reduce the heat flux near the divertor plate. Furthermore, the radiation-cooling rate of Xe is much higher compared to other noble gases at the temperature range a few eV to hundred keV. That could be a

author's e-mail: islam.mdshahinul@nifs.ac.jp, shahinulislamrony@gmail.com

strong point as a radiator gas in divertor. Xe gas is shown to be the most effective radiator for generating detached plasma in the D-module of GAMMA 10/PDX [6]. Transition phenomenon of plasma detachment during the additional heating effect has been recently started in GAMMA 10/PDX [7]. During transient heating condition, the distribution of plasma parameters on the target plate has not been studied in the previous study [7]. In this paper, the detailed plasma parameters on the target plate are studied to understand the impact of transient heating pulse on the detached plasma. The 27 m long GAMMA 10/PDX consists of a central-cell, two anchor-cells, two plug/barrier-cells, and two end-cells. The plasma heating and confinement are performed at the central-cell. The plasma heating tools such as Neutral Beam Injection (NBI), Ion Cyclotron Range of Frequency (ICRF), and Electron Cyclotron Heating (ECH) have been installed on the GAMMA 10/PDX to heat the plasma. By using the end-loss plasma, the divertor simulation research is performed at the west end-cell of the device [6–10]. A numerical simulation study is also performed by using the LINDA code [11–16].

In this paper, we investigate the transient response of heat pulse (ELM like) on the detached state by applying the ECH. More specifically, the present paper investigates the influence of the ECH heating for interrupting the detached plasma at the D-module of GAMMA 10/PDX.

2. Experimental Setup

The schematic drawing of the central-cell to end-cells of the GAMMA 10/PDX machine are given in Fig. 1. The GAMMA 10/PDX has several heating systems as shown in Fig. 1. In a typical plasma experiment, the initial hydrogen plasmas are seeded by the magneto-plasma-dynamic (MPD) arc jet plasma guns, which have been installed at both ends of the device. The plasmas are heated and sustained in the central-cell by gas puffing and ICRF (RF1-RF2) heating. The double half-turn (DHT) antennas and the Nagoya Type-III antennas are installed at the east and the west side of the central-cell, as shown in Fig. 1. In a typical ICRF-heated plasma discharge, the first ICRF system (RF1) has been used for the plasma production in the central-cell and the MHD stabilization in the anchor-cell. On the other hand, the second ICRF (RF2) system has been used for ion heating in the central-cell. More detailed descriptions of the ICRF heating systems and positions of the antennas are given in the Refs. [17–19]. The effective input heating power ($P_{\mathrm{input}} - P_{\mathrm{reflected}}$) of the RF1 antennas were 100 kW and 80 kW, respectively. On the contrary, the effective input power of the RF2 antennas were 70 kW, and 60 kW, respectively. Thus, the total ICRF input effective heating power is 310 kW. The heating ratio of the ECH power to the ICRF power is estimated to be 0.3225 (100 kW/310 kW).

The divertor simulation experimental module (D-module) has been designed at the west end-cell of the device, as shown in Figs. 1 and 2. An elevation system is used in order to conduct both the conventional mirror experiments and the D-module experiments. During the D-module experiments, the D-module has been adjusted on the axis and the initial seed hydrogen plasma is seeded by using only the east side plasma gun. As shown in Fig. 2, the cross-section area and the length of the D-module are 50 × 50 cm and 70 cm, respectively. Figure 3 (a) shows the schematic view of the D-module. The D-module is designed with (1) a rectangular chamber, (2) a V-shaped tungsten target, and (3) a gas injection system. The schematic drawing of the V-shaped target is given in Fig. 3 (b). Two target plates (350 × 300 mm) made of tungsten have been designed in V-shape inside the D-module.

The angle of the two plates can vary from 15 to 80 degrees. As shown in Fig. 3 (b), several types of gas seeding systems are installed in the module. As shown in Fig. 3 (a),

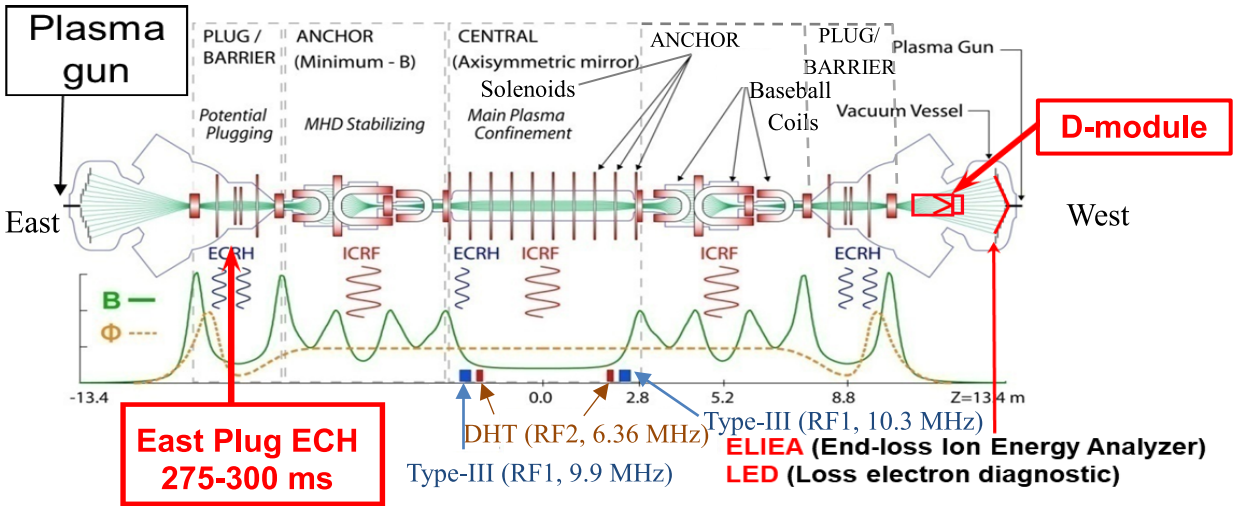

Fig. 1 Schematic view of the GAMMA 10/PDX tandem mirror device.

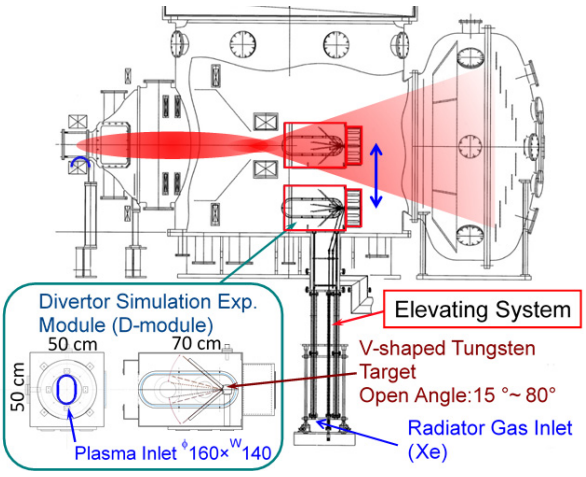

Fig. 2 Schematic view of the GAMMA 10/PDX west-end cell, and D-module.

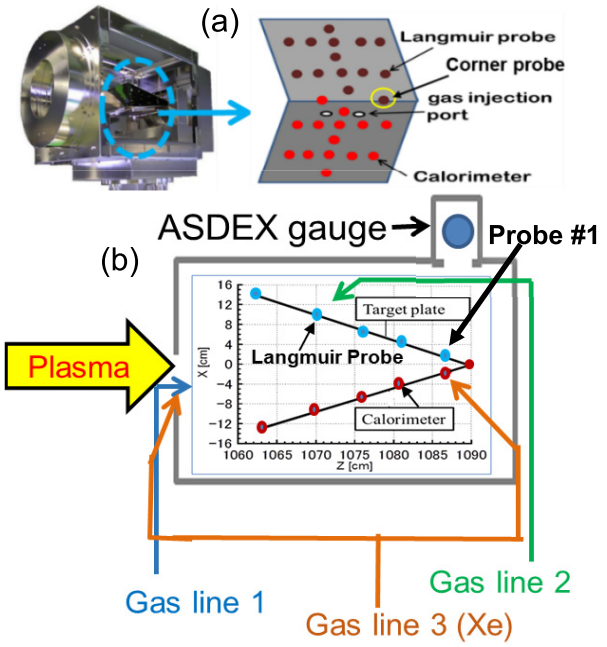

Fig. 3 Schematic view of (a) D-module, and (b) gas injection system.

thirteen calorimeters and Langmuir probes are also located at the lower and the upper plates of the target, respectively. Furthermore, a calorimeter and a probe have been also installed inside the gap of the target plate. These probes and calorimeters are installed along the target plate but not along the magnetic field line. Therefore, the variation of plasma parameters and averaged heat fluxes measured by the probes and calorimeters show the radial profiles of plasma parameters and heat fluxes. In this experiment, the distribution of plasma parameters on the target plate was measured under the target angle of 45 degrees. In the present experiment, Xe gas injection was carried out into the D-module through gas line#3. Xe gas was injected 0.8 s earlier than the plasma discharge due to the low conductance of the gas seeding system. The gas was puffed until the end of the plasma discharge. Therefore, the gas was distributed uniformly in the D-module. At present, Xe gas injection into the D-module has been controlled by varying the plenum pressure of the gas reservoir tank. In this experiment, the Xe gas injection was carried out in the range of plenum pressure of 0 to 30 kPa. The plasma parameters in the central-cell are affected significantly when higher Xe gas is injected.

3. Experimental Results and Discussion

During detached plasma formation experiments by Xe seeding, a pulse (275 - 300 ms) of ECH has been applied at the east plug-cell to increase plasma flux at the end-cell. The injection position of the ECH heating power is shown in Fig. 1. The ECH injection on the east plug cell enhances the warm electron flow to the central-cell [7], which may enhance ionization of neutral particles at the D-module.

3.1 Electron temperature and current at the west end-cell plate during the ECH heating

The electron temperature, and electron current at the west end-cell plate are measured by the Loss Electron Diagnostics (LED) [20], when D-module moves below the vacuum chamber of GAMMA 10/PDX. The energy spectra of the end-loss electrons have not been evaluated using a single component Maxwellian. However, the electron current measured by the LED has been well fitted to a two-component Maxwellian, as written below:

$$I_e = I_{eL} \exp\left(-\frac{V_{ER}+\phi_{EP}}{T_{eL}}\right) + I_{eH} \exp\left(-\frac{V_{ER}+\phi_{EP}}{T_{eH}}\right). \quad (1)$$

Here, V_{ER} is the electron repeller voltage and ϕ_{EP} represents the end-plate potential ($\phi_{EP} < 0$). I_{eL} and I_{eH} represent electron current of lower and higher component, respectively. T_{eL} and T_{eH} denote the temperature of the bulk warm component and the high-energy tail component, respectively. Using these parameters, an effective electron temperature ($T_{e-effective}$) is defined as the measure of the mean energy as follows:

$$T_{\text{e-effective}} = (1-\beta)T_{eL} + \beta T_{eH}. \quad (2)$$

Where, β is the flux fraction component to the total flux: $\beta = \frac{I_{eH}}{I_{eL}+I_{eH}}$. More details are given in Refs. [20, 21].

Figure 4 shows the dependence of effective electron and ion temperature at the west end-cell plate as a function of ECH heating power. As shown in Fig. 4 (a), $T_{e-effective}$ increases significantly during ECH heating. The β is estimated to be 0.317 and 0.555 for the ECH heating power of 100 and 150 kW, respectively. The ECH heating pulse significantly increases T_{eH}, as shown in Fig. 4 (a). On the other hand, the T_{eL} moderately increases under the ECH

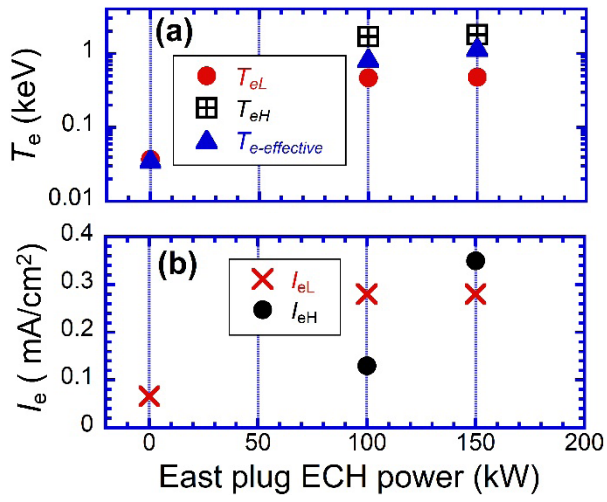

Fig. 4 Dependence of electron temperature and current measured by the LED at the west end-cell plate.

pulse (see Fig. 4 (a)). However, the power dependence of ECH on the T_{eH} and T_{eL} has not been observed in the experiment, as shown in Fig. 4 (a).

The electron current is shown in Fig. 4 (b). The I_{eL} and I_{eH} are enhanced during ECH heating pulse (see Fig. 4 (b)). Furthermore, the I_{eL} is shown to be similar for the ECH heating power of 100 kW and 100 kW, as shown in Fig. 4 (b). On the contrary, the I_{eH} is enhanced significantly with increasing ECH power 100 kW to 150 kW, as shown in Fig. 4 (b). These outcomes represent the impact of ECH heating on the west end-cell plasma parameters.

3.2 Impact of ECH heating on the upstream and downstream plasma parameters

The electron line density (NLcc) at the central-cell has been measured by the microwave interferometer [22]. The average electron line density ($n_{\text{e–av.}}$) has been calculated by dividing the NLcc by the plasma diameter ($\phi \sim 36$ cm). The calculated $n_{\text{e–av.}}$ at the central-cell is shown in Fig. 5 (a). As shown in Fig. 5 (a), the $n_{\text{e–av.}}$ increases slightly when ECH is applied. The ECH application period is highlighted by the yellow color in Fig. 5. Furthermore, the $n_{\text{e–av.}}$ slightly increases during Xe injection cases, as shown in Figs. 5 (a) and (c). As the Xe gas pressure increases, so does the density. The $n_{\text{e–av.}}$ remains almost stable during Xe injection into the D-module (see Fig. 1), which indicates that reproducibility of the central-cell plasmas was not affected significantly due to the Xe injection.

Figure 5 (b) shows the time response of the ion saturation current (I_{i-sat}). Without ECH injection time, the I_{i-sat} reduces drastically with increasing Xe injection into the D-module, as shown in Fig. 5 (b). On the other hand, the I_{i-sat} at the corner of the D-module increases abruptly with increasing Xe injection in the case of the ECH heating period (highlighted parts in Fig. 5 (b)). The I_{i-sat} increases

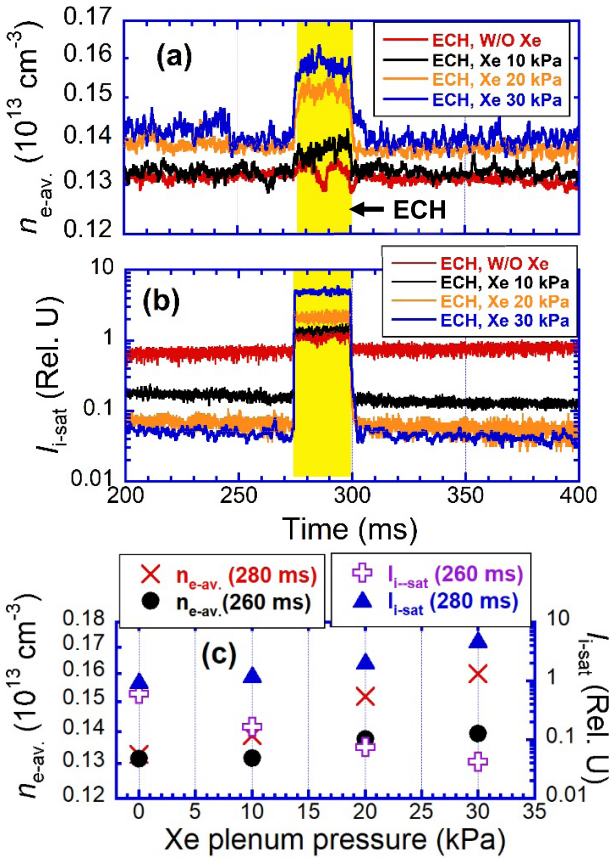

Fig. 5 Time behavior of (a) $n_{\text{e–av.}}$ measured at the central-cell, (b) I_{i-sat} (corner probe) at the D-module in the case of ECH 100 kW, and (c) dependence of $n_{\text{e–av.}}$ and I_{i-sat} as a function of Xe plenum pressure.

remarkably with changing the gas reservoir plenum pressure 20 to 30 kPa, as shown in Fig. 5 (b).

As shown in Fig. 5 (c), the $n_{\text{e–av.}}$ is increased with increasing Xe plenum pressure for both the ECH (at 280 ms) and without ECH (260 ms) cases. However, the increasing rate in $n_{\text{e–av.}}$ is higher with increasing Xe plenum pressure during ECH injection, as shown in Fig. 5 (c). For the case of without ECH injection (260 ms), I_{i-sat} is reduced drastically with increasing Xe injection (see Fig. 5 (c)). On the other hand, during ECH injection case (280 ms), I_{i-sat} is enhanced significantly with increasing Xe plenum pressure, as shown in Fig. 5 (c).

The reason for such drastic increase in I_{i-sat} is not clearly understood. However, it is speculated that the ionization of neutral particles increases with increasing gas pressure, which induces such drastic increases in the ion flux. It is clearly observed that the application of ECH on the east plug-cell drastically influences the ion saturation current in the D-module.

The dependence of ECH heating power and Xe plenum pressure on the ion saturation current at the corner of the D-module is investigated and shown in Fig. 6. The particle flux on the target plate can be expressed as follows:

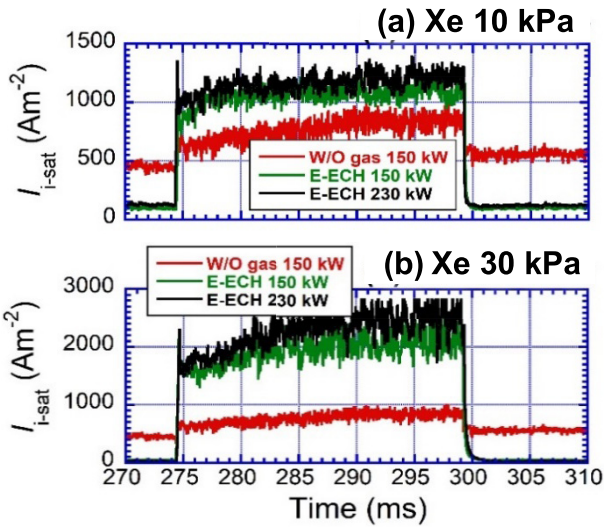

Fig. 6 Time behavior of ion saturation current (corner probe) at the D-module for (a) Xe 10 kPa, and (b) Xe 30 kPa.

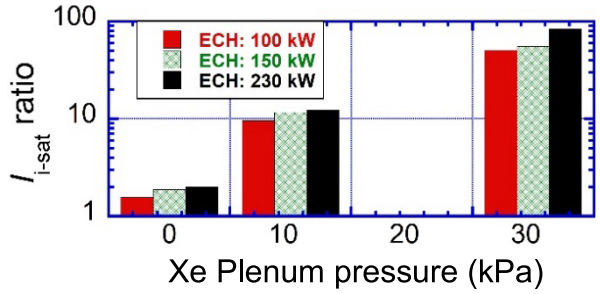

Fig. 7 Increase ratio of the ion flux for 295 ms and 270 ms.

$$\Gamma_{\mathrm{d}} = \Gamma_{\mathrm{upstream}} - \Gamma_{sink} + \Gamma_{source}. \quad (3)$$

Where, Γ_{d} is the particle flux on the target plate, $\Gamma_{\mathrm{upstream}}$ is the upstream plasma flux entering to the divertor region. Γ_{sink} and Γ_{source} represent the sink and source terms in the divertor region. Hence, the particle flux on the target plate can be reduced by either reducing upstream and source terms or increasing sink terms. As shown in Fig. 6, during ECH injection time, the ion saturation current enhances significantly with increasing the amount of Xe injection. Compared to Fig. 6 (a) and Fig. 6 (b), the ion flux increases slightly with increasing ECH heating power. In particular, the ion saturation current is enhanced remarkably when Xe injection is increased from 10 kPa to 30 kPa, as shown in Fig. 6. However, the upstream plasmas density is affected slightly with increasing Xe injection from 10 kPa to 30 kPa, as shown in Fig. 5 (a). The increase ratio of the ion flux is shown in Fig. 7. As shown in the figure, for without Xe injection case, the ion flux is increased by approximately 2 times by the ECH heating pulse, which indicates the effect of the ECH heating pulse. The power dependence of ECH power on the ion flux is small, as shown in Fig. 7. On the contrary, the ion flux increases

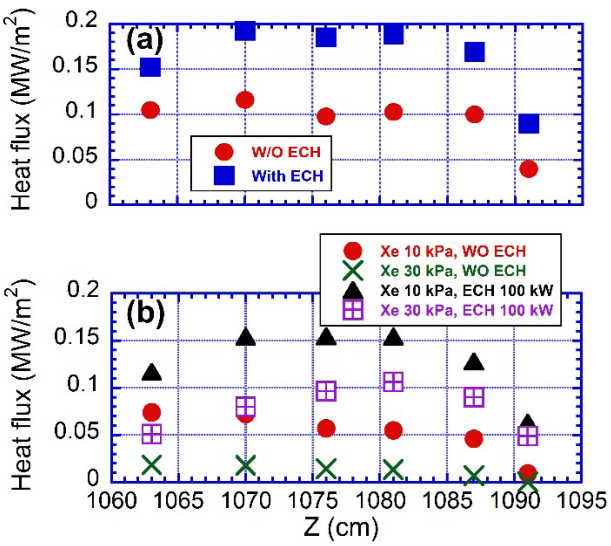

Fig. 8 Dependence of heat flux on the target plate (a) without Xe, and (b) with Xe injection.

drastically during Xe injection (see Fig. 7). In addition, the increase ratio of ion flux increases with the increment of Xe plenum pressure, as shown in Fig. 7. As a result, the amount of Xe gas plays a dominant role for enhancing ion flux during the ECH heating pulse. The reason for increasing the ion saturation current due to the ECH heating effect produces warm electrons flow toward the D-module, which enhances ionization in the D-module. This factor affects the plasma and neutral particles in the D-module. In the future, we will design a probe and a calorimeter in front of the target plate to clarify the particle balance and spatial distribution of detached plasma in the D-module of GAMMA 10/PDX.

3.3 The heat flux, electron density and temperature on the V-shaped target

The heat flux is measured by the calorimeter. The heat flux is evaluated by the thermocouple. More specifically, the heat flux is evaluated by comparing the temperature difference (ΔT) between before and after plasma discharge [23]. Therefore, we cannot measure the time resolved value of the heat flux by calorimeter. In this paper, we report the time averaging value of the heat flux for the full plasma discharge (400 ms). Since the magnetic field lines are expanding at the end-cell of GAMMA 10/PDX, the magnetic field is different on the heat flux measuring positions. The Z-axial position of the calorimeters represents the Z-axial position from the central-cell [23].

The distribution of the heat flux along the target plate of the module is shown in Fig. 8. The variation in Fig. 8 (a) comes from the configuration of the magnetic field structure at the end-region of GAMMA 10/PDX. More detailed explanation has been reported in Ref. [13]. As shown in Fig. 8, the heat flux reduces along the target plate during Xe injection (without ECH injection) but this tendency

changes in the case of the ECH heating condition. During ECH injection case, the heat flux slightly increases from the inlet measuring position (Z = 1063 cm) to Z = 1076 cm (see Figs. 8 (a) - (b)). As shown in Figs. 4 and 5, the ECH injection changes plasma flux and electron temperature significantly, which strongly affects neutral-plasma collisions in D-module. The heat flux is the product of plasma density, temperature, and velocity. The electron density increases due to the ionization of the neutral particles. We will discuss the density and temperature profile on the target plate in the next sub-section to clarify the heat flux profile. The plasma velocity has not yet been measured in the D-module to date. As shown in Fig. 8 (b), Xe injection significantly reduces the heat flux on the target plate for only ICRF heated plasma (P_H^{woECH}). On the other hand, for additional heating cases, the heat flux reduces slightly on the target plate, as shown in Fig. 8. In particular, the increase ratio of the heat flux $(P_H^{ECH} - P_H^{woECH})/P_H^{ECH}$ for ECH and without ECH (only ICRF heated plasma) increases with the increasing Xe plenum pressure. From Fig. 8 (a) and Fig. 8 (b), once Xe is injected, the heat flux reduces significantly but the ECH heating effect increases the heat flux even though the injected ECH power is small. Hence, it is important to consider the effect of high heat flux on the sustainment of detached plasma.

In order to clarify the effect of ECH and Xe pressure, the dependence of electron density (n_e) and electron temperature (T_e) as a function of Xe plenum pressure is shown in Fig. 9. As shown in Fig. 9, during the without ECH injection case, the n_e shows a roll-over phenomenon with increasing Xe gas injection. A roll-over in the n_e is one of the most important symptoms of detached plasma formation. Consequently, a detached plasma is observed by Xe seeding for the case of without ECH injection. On the contrary, in the case of ECH injection, the n_e is increased remarkably with increasing Xe injection, as shown in Fig. 9. During the ECH injection case, a roll-over phenomenon in the n_e has not been shown in Fig. 9, which indicates that the ionization process is still active.

In the experiment, we could not properly measure the T_e during the ECH time. As shown in Fig. 9, T_e is reduced drastically with increasing Xe plenum pressure for the case of without ECH case. In particular, for the Xe 20 kPa injection case, T_e is reduced lower to 1.6 eV. Since the T_e is reduced significantly, the recombination processes dominate the ionization processes. As a consequence, a roll-over phenomenon is observed in n_e (see Fig. 9). The electron energy loss channels (ionization, excitation, radiation) enhance with the increment of Xe gas throughput into the D-module, which strongly reduces the T_e in the D-module.

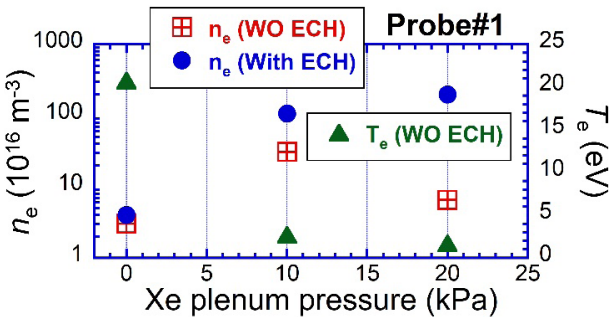

Fig. 9 Dependence of electron density and temperature measured by probe #1 as a function of Xe plenum pressure.

3.4 2D visible emission from V-shaped target

The two-dimensional images of the visible emission (without filter) are captured by the high-speed camera. The high-speed camera has been located on the horizontal port for capturing the visible emission from the D-module. For Xe 10 kPa injection case, the detached plasma is not formed, as discussed in Sec. 3.3. Consequently, bright region appears in whole region of D-module for Xe 10 kPa injection, as shown in Fig. 10 (a). As shown in Fig. 10 (a), during ECH injection period a bright emission appears close to the corner of the target for Xe 30 kPa injection case, which represents ionization effect of Xe particles due to abrupt changes in upstream plasma parameters. Since the Xe gas is seeded from the inlet and the corner of the target (gas line #3), neutral particles may concentrate close to the target plate when plasma becomes detached. As shown in Figs. 4 - 5, the upstream and downstream plasma parameters are significantly affected by the ECH heating pulse, which ionize the Xe neutral particles in the D-module. Xe neutral density is higher close to the gas seeding ports. As a result, a bright emission appears close to the corner, as shown in Fig. 10 (a). Moreover, dark region appears at the later part of plasma discharge for Xe 30 kPa injection. Figure 10 shows the visible emission from plasma and neutral particles. For without ECH heating case, the visible emission from the D-module is significantly reduced when Xe plenum pressure increased from 10 kPa to 30 kPa, as shown in Fig. 10 (b).

3.5 Discussion

In the present study, the effects of ECH heating on the detached plasma has been investigated based on the Langmuir probes, high-speed camera, and calorimeters measurements. The plasma detachment state has been shown for Xe seeding in the cases of only ICRF heated plasma. However, the detached state has not been sustained for the ECH heating cases.

Plasma energy can be reduced by the ionization, excitation, radiative power loss, charge-exchange (CX) loss, momentum loss, and volume recombination. The volumetric recombination processes (EIR and MAR) lead to play a role as the electron temperature is decreased, which also induces a reduction in the ion and heat fluxes.

Impurity gas injection increases both the ions and the electron density by ionization. This effect also influences

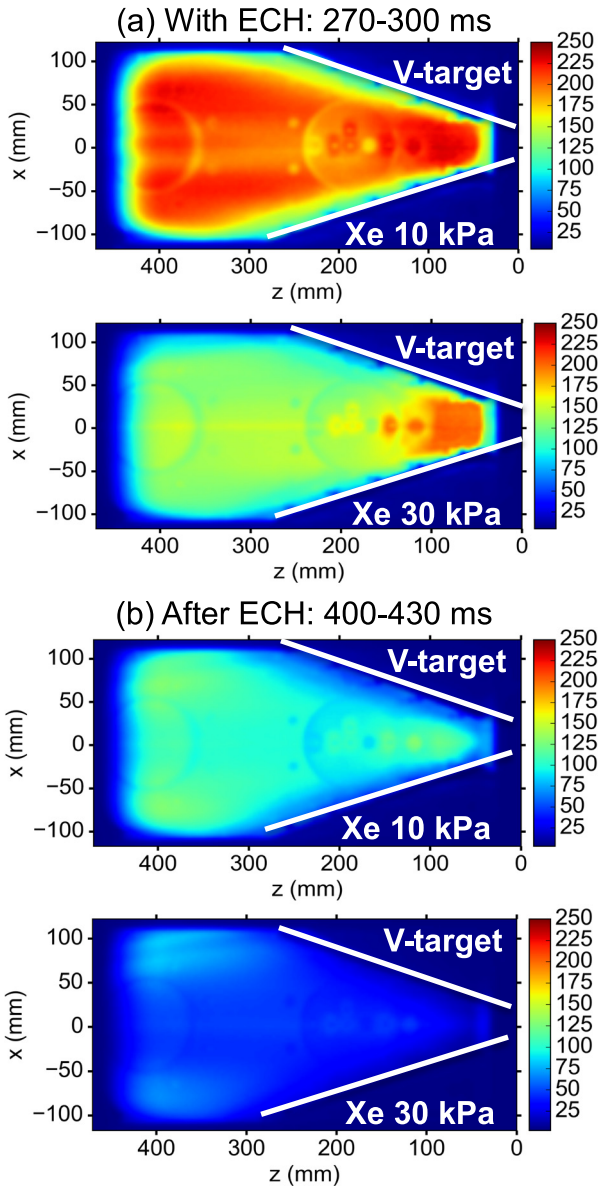

Fig. 10 2D image of visible emission from the D-module was captured by the high-speed camera (a) with ECH (100 kW) and (b) after ECH injection period.

the plasma density and temperature. The radiative power loss and ionization might be the main energy loss processes for electrons while CX loss and electron-ion relaxation are the main energy loss processes for ion. The radiation power loss and the ionization loss represent the energy loss mechanism during interaction of electron and impurity particles. As the electron energy is reduced, the ion energy is also reduced by the electron-ion relaxation processes.

In this experiment, for only ICRF heated plasma, Xe injection into the GAMMA 10/PDX has shown a promising effect on the reduction of the electron temperature, heat flux, and ion flux, which implies that the formation of a detached plasma. The ECH application at the east plug-cell significantly enhances the warm electron temperature at the west end-cell. Consequently, during the additional ECH transient heating pulse, the ion flux in the D-module is significantly enhanced via the ionization and excitation of neutral particles. Moreover, the ion flux in the D-module is enhanced with increasing the Xe gas throughput in the D-module, which clearly indicates the ionization processes of Xe play a key role during the ECH application period.

From the above discussion, it has been clarified that heavy noble gas Xe can be easily ionized during an additional heating case in spite of the strong impact on achieving plasma detachment, which drives the detached plasma towards attached plasma. It is mandatory to sustain the detached plasma during the transient heating pulse (such as ELMs in tokamak). However, the present study shows that the detached plasma was not sustained during the transient ECH heating pulse. More detailed experiments and discussion are necessary to clarify the reported phenomenology. It is necessary to examine the impact of Ne, N_2, and simultaneous injection of N_2 + H_2 on the sustainability of the detached plasma.

4. Summary

The transient behavior of detached plasma in the D-module has been investigated by applying an ECH heating pulse at the upstream region. The ECH heating pulse significantly increases high-energy tail component toward the west end-cell. It is shown that the transient heating effect of ECH significantly affects the plasma parameters in the D-module. The electron density increases abruptly for the ECH heating case. The heat and ion fluxes increase significantly for the ECH injection case, which clearly represents the transition of detached to attached state by the ECH heating pulse. From the above discussion, the transient heating pulse may be a promising method for investigating the detached to attached transition phenomena in divertor studies.

Acknowledgments

This study was supported by the bidirectional collaboration research program of the University of Tsukuba, and National Institute for Fusion Science (NIFS19KUGM140). The authors would like to thank the members of the GAMMA 10 group for their support during the experiment.

[1] P.C. Stangeby, Plasma Phys. Control. Fusion **43**, 223 (2000).
[2] A. Loarte *et al.*, Nucl. Fusion **47**, S203 (2007).
[3] A. Kallenbach *et al.*, Plasma Phys. Control. Fusion **58**, 045013 (2016).
[4] S. Takamura *et al.*, J. Plasma Fusion Res. **4**, 138 (2001).
[5] N. Ohno, Plasma Phys. Control. Fusion **59**, 034007 (2017).
[6] Y. Nakashima *et al.*, Nucl. Fusion **57**, 116033 (2017).
[7] Y. Nakashima *et al.*, Nucl. Mater. Energy **18**, 216 (2019).
[8] N. Ezumi *et al.*, Nucl. Fusion **59**, 066030 (2019).
[9] M.S. Islam *et al.*, Plasma Fusion Res. **11**, 2402042 (2016).
[10] M.S. Islam *et al.*, Plasma Fusion Res. **14**, 2402016 (2019).

[11] M.S. Islam *et al.*, Nucl. Mater. Energy **18**, 182 (2019).
[12] M.S. Islam *et al.*, Plasma Phys. Control. Fusion **59**, 125010 (2017).
[13] M.S. Islam *et al.*, Plasma Phys. Control. Fusion **61**, 125005 (2019).
[14] M.S. Islam *et al.*, Plasma Fusion Res. **13**, 3403080 (2018).
[15] M.S. Islam *et al.*, Contrib. Plasma Phys. **58**, 805 (2018).
[16] M.S. Islam *et al.*, Fusion Eng. Des. **125**, 216 (2017).
[17] T. Yokoyama *et al.*, Plasma Fusion Res. **7**, 2402136 (2012).
[18] Y. Yamaguchi *et al.*, Plasma Phys. Control. Fusion **48**, 1155 (2006).
[19] M. Hirata *et al.*, Plasma Fusion Res. **14**, 2402055 (2019).
[20] K. Kurihara *et al.*, J. Phys. Soc. Jpn **58**, 3453 (1989).
[21] R. Minami *et al.*, Plasma Fusion Res. **14**, 2402034 (2019).
[22] J. Kohagura *et al.*, Fusion Sci. Technol. **63**, 176 (2013).
[23] M. Iwamoto *et al.*, Plasma Fusion Res. **9**, 3402121 (2014).